

PREPARED FOR SUBMISSION TO JHEP

The chiral transition in a magnetic background: Finite density effects and the functional renormalization group

Jens O. Andersen^{a,b} Anders Tranberg^b

^a*Department of Physics, Norwegian University of Science and Technology, Høgskoleringen 5, N-7491 Trondheim, Norway*

^b*Niels Bohr International Academy, Niels Bohr Institute and Discovery Center, Blegdamsvej 17, DK-2100 Copenhagen, Denmark*

E-mail: andersen@tf.phys.ntnu.no, anders.tranberg@nbi.dk

ABSTRACT: We compute the phase diagram of the quark-meson model at finite temperature, finite baryon chemical potential $\mu_B = 3\mu$ and constant external magnetic field B , using the functional renormalization group. Our results show that the critical temperature increases as a function of B at $\mu = 0$, but for values μ larger than about 210 – 225 MeV, the opposite behavior is realized. As the magnetic field increases, the critical point (T^*, μ^*) moves from large μ , small T towards small μ , larger T in the μ – T phase diagram.

KEYWORDS: Finite-temperature field theory, chiral transition, magnetic field

Contents

1	Introduction	1
2	Quark-meson model and the functional renormalization group	3
3	Numerical results	4
4	Discussion and conclusion	9
A	Flow equation	11

1 Introduction

The phase structure of QCD as a function of temperature T and baryon chemical μ_B has received a lot of attention. This interest has been spurred by the ongoing heavy-ion collision experiments at RHIC (Brookhaven) and the LHC (CERN) and the search for the location of the critical endpoint where the curve of first-order chiral transitions terminates. Moreover, it turns out that the phase diagram has a much richer structure than was anticipated. In particular, there are a number of color superconducting phases at large baryon chemical potential and low temperature (see for example the reviews [1, 2] for a thorough discussion). More recently, there has been quite some interest in the behavior of strongly interacting matter in external electromagnetic fields, motivated by astrophysical phenomena as well as heavy-ion collisions. Large magnetic fields exist inside ordinary neutron stars as well as magnetars [3]. Similarly, strong, but short-lived magnetic fields, up to $B \sim 10^{19}$ Gauss or $|qB| \sim 6m_\pi^2$, may be generated during noncentral heavy-ion collisions at RHIC and LHC [4–6]. In the context of strongly interacting matter in an external magnetic field, at least three important questions have arisen: Does the order of the transition change with the strength of the magnetic field B ?; how does the critical temperature T_c depend on the strength of the magnetic field B ?; and is there a splitting between the chiral transition and the deconfinement transition beyond some finite value of the B -field? We will address the first two of these questions in the present work.

In Ref. [7] chiral perturbation theory at leading order was used to study the chiral transition as a function of magnetic field. Comparing the pressure of a hot pion gas with that of a noninteracting quark-gluon plasma with a subtracted vacuum energy term due to a nonzero gluon condensate, they found a first-order transition for weak magnetic fields. The line of first-order transitions ends at a critical point $(\sqrt{|qB|}, T) = (600, 104)$ MeV, where $|q|$ is the pion electric charge. For larger values of $|qB|$, the transition is a crossover.

The authors of Ref. [8] use the Polyakov loop extended quark-meson (QM) model to study the phase transition. The bosons are treated at tree level while the fermions are treated at the one-loop level, except that the vacuum fluctuations at zero magnetic field are neglected. The authors report

that they find a first-order transition at the physical point if they keep the remaining B -dependent vacuum fluctuations and a crossover if they are ignored. The mean-field calculations of Ref. [9] as well as the functional renormalization group calculation of Ref. [10] using the QM model suggest that the transition remains a crossover. The conflicting result between Ref. [8] and Refs. [9, 10] could be due to a different treatment of the vacuum fluctuations. In Refs. [11, 12] the effects of the vacuum fluctuations on the chiral transition were studied for $B = 0$, and it was shown that both the critical temperature T_c and the order of transition depend on whether they are included or not.

Most model calculations conclude that the critical temperature is an increasing function of the magnetic field B . This includes both mean-field type calculations [8, 13–20] involving (Polyakov-loop extended) Nambu-Jona-Lasinio (NJL) and quark-mesons models as well as chiral perturbation theory, and beyond mean field using functional renormalization group techniques [10]. These results are in line with the lattice calculations of Refs. [22, 23], however, these were carried out for bare quark masses that correspond to very large pion masses in the 200–480 MeV range. The very recent simulations of Bali *et al* [24, 25] for a pion mass of 140 MeV as well the MIT-bag calculations of Ref. [26] suggest that the critical temperature decreases with the strength of the magnetic field.

In order to address the issue of whether there is a splitting between the chiral and deconfinement transitions, one must go beyond the NJL or QM models since these have nothing to say about the latter. This can be done by introducing an effective phenomenological potential for a constant temporal gluon field and expressing it in terms of the thermal expectation value of the trace of the Polyakov loop [27]. The conclusion of Ref. [8] is that the deconfinement transition temperature decreases with the strength of the magnetic field, while the chiral transition temperature increases. Similar conclusions were reached in [10], where a functional renormalization-group approach was used together with the P(QM) model to include mesonic fluctuations in the calculations.

In the present paper, we continue to explore the properties of QCD in an external magnetic field using the quark-meson model. The work is a continuation of Ref. [9] in which the phase diagram in the μ – T plane was mapped out for strong fields, $|qB| \sim 5m_\pi^2$. The calculations were carried out in the mean-field approximation and the large- N_c limit where the bosonic modes are treated at tree level. Moreover, the influence of the fermionic vacuum fluctuations on the transition was studied. In the chiral limit, it was found that the transition is first order in the entire μ – T plane if vacuum fluctuations are not included and second order if they are included. Here we are using the functional renormalization group (FRG) [28] to investigate the behavior of strongly interacting matter in a magnetic background. The functional renormalization group is a non-perturbative, self-consistent resummation, with a wide range of applicability. See for example [30] for a recent review.

The paper is organized as follows. In Sec. 2, we briefly discuss the quark-meson model and the functional renormalization group. In Sec. 3, we present and discuss our numerical results while we summarize in Sec. 4. The renormalization group equation for the effective potential is derived in Appendix A.

2 Quark-meson model and the functional renormalization group

The $O(4)$ -invariant Euclidean Lagrangian for the quark-meson model is

$$\begin{aligned} \mathcal{L} = & \bar{\psi} \left[\gamma_\mu \partial_\mu - \mu \gamma_4 + g(\sigma - i\gamma_5 \boldsymbol{\tau} \cdot \boldsymbol{\pi}) \right] \psi + \frac{1}{2} \left[(\partial_\mu \sigma)^2 + (\partial_\mu \boldsymbol{\pi})^2 \right] + \frac{1}{2} m^2 \left[\sigma^2 + \boldsymbol{\pi}^2 \right] \\ & + \frac{\lambda}{24} \left[\sigma^2 + \boldsymbol{\pi}^2 \right]^2 - h\sigma, \end{aligned} \quad (2.1)$$

where σ is the sigma field, $\boldsymbol{\pi}$ denotes the neutral and charged pions. $\boldsymbol{\tau}$ are the Pauli matrices, $\mu = \frac{1}{2}(\mu_u + \mu_d)$ is the quark chemical potential, in terms of μ_u and μ_d , the chemical potential for the u and d quarks, respectively. The baryon chemical potential is given by $\mu_B = 3\mu$. We set $\mu_u = \mu_d$ so that we are working at zero isospin chemical potential, $\mu_I = \frac{1}{2}(\mu_u - \mu_d) = 0$. The Euclidean γ matrices are given by $\gamma_j = i\gamma_M^j$, $\gamma_4 = \gamma_M^0$, and $\gamma_5 = -\gamma_M^5$, where the index M denotes Minkowski space. The fermion field is an isospin doublet

$$\psi = \begin{pmatrix} u \\ d \end{pmatrix}. \quad (2.2)$$

If $h = 0$, Eq. (2.1) is invariant under $O(4)$. If $h \neq 0$, chiral symmetry is explicitly broken, otherwise it is spontaneously broken in the vacuum. Either way, the symmetry is reduced to $O(3)$. Note that this requires $m^2 < 0$ which is assumed in the remainder of the paper.

Chiral symmetry is broken in the vacuum by a nonzero expectation value ϕ for the sigma field and we make the replacement

$$\sigma \rightarrow \phi + \tilde{\sigma}, \quad (2.3)$$

where $\tilde{\sigma}$ is a quantum fluctuating field. The tree-level potential then becomes

$$U_\Lambda = \frac{1}{2} m_\Lambda^2 \phi^2 + \frac{\lambda_\Lambda}{24} \phi^4 - h\phi. \quad (2.4)$$

Note that we have introduced a subscript Λ on U , m^2 , and λ , where Λ is the ultraviolet cutoff of the theory (see section 3). This is a reminder that these are unrenormalized quantities ¹.

We will follow Wetterich's implementation of the renormalization group ideas based on the effective average action $\Gamma_k[\phi]$ [28]. This action is a functional of a set of background fields that are denoted by ϕ . $\Gamma_k[\phi]$ satisfies an (integro-differential) flow equation in the variable k , to be specified below. The subscript k indicates that all the modes p between the ultraviolet cutoff Λ of the theory and k have been integrated out. When $k = \Lambda$ no modes have been integrated out and Γ_Λ equals the classical action S . On the other hand, when $k = 0$, all the momentum modes have been integrated out and Γ_0 equals the full quantum effective action. The flow equation then describes the "flow" in the space of effective actions as a function of k .

In order to implement the renormalization group ideas, one introduces a regulator function $R_k(p)$. The function $R_k(p)$ is large for $p < k$ and small for $p > k$ whenever $0 < k < \Lambda$, and $R_\Lambda(p) = \infty$.

¹ The symmetry breaking term is equivalent to an external field that does not flow and therefore $h = h_\Lambda$.

These properties ensure that the modes below k are heavy and decouple, and only the modes between k and the UV cutoff Λ are light and integrated out. The choice of regulator function has been discussed in detail in the literature and some choices are better than others due both to their analytical and stability properties. We briefly discuss our choice of regulator in Appendix A.

The flow equation for the effective action cannot be solved exactly so one must make tractable and yet physically sound approximations. The first approximation in a derivative expansion is the local-potential approximation and in this case the flow equation for Γ_k reduces to a flow equation for an effective potential $U_k(\phi)$. In the case of a constant magnetic field, the differential equation for U_k reads [10]

$$\begin{aligned} \partial_k U_k = & \frac{k^4}{12\pi^2} \left\{ \frac{1}{\omega_{1,k}} [1 + 2n_B(\omega_{1,k})] + \frac{1}{\omega_{k,2}} [1 + 2n_B(\omega_{2,k})] \right\} \\ & + k \frac{|qB|}{2\pi^2} \sum_{m=0}^{\infty} \frac{1}{\omega_{1,k}} \sqrt{k^2 - p_{\perp}^2(q, m, 0)} \theta(k^2 - p_{\perp}^2(q, m, 0)) [1 + 2n_B(\omega_{1,k})] \\ & - \frac{N_c}{2\pi^2} k \sum_{s,f,m=0}^{\infty} \frac{|q_f B|}{\omega_{q,k}} \sqrt{k^2 - p_{\perp}^2(q_f, m, s)} \theta(k^2 - p_{\perp}^2(q_f, m, s)) [1 - n_F^+(\omega_{q,k}) - n_F^-(\omega_{q,k})] , \end{aligned} \quad (2.5)$$

where we have defined $\omega_{1,k} = \sqrt{k^2 + U_k}$, $\omega_{2,k} = \sqrt{k^2 + U' + 2U_k''\rho}$, $\omega_{q,k} = \sqrt{k^2 + 2g^2\rho}$, $p_{\perp}^2(q, m, s) = (2m + 1 - s)|qB|$, $n_B(x) = 1/(e^{\beta x} - 1)$, $n_F^{\pm}(x) = 1/(e^{\beta(x \pm \mu)} + 1)$, and $\rho = \frac{1}{2}\phi^2$. We briefly discuss the derivation of Eq. (2.5) in Appendix A. If we neglect the bosonic fluctuations by ignoring the first two lines of Eq. (2.5), we can solve the equation for U_k analytically. This yields the standard mean-field result for the one-loop thermodynamic potential [9].

At zero temperature, the Bose distribution function vanishes and the Fermi distribution function becomes a step function. The flow equation (2.5) then reduces to

$$\begin{aligned} \partial_k U_k = & \frac{k^4}{12\pi^2} \left\{ \frac{1}{\omega_{1,k}} + \frac{1}{\omega_{2,k}} \right\} + k \frac{|qB|}{2\pi^2} \sum_{m=0}^{\infty} \sqrt{k^2 - p_{\perp}^2(q, m, 0)} \theta(k^2 - p_{\perp}^2(q, m, 0)) \\ & - \frac{N_c}{2\pi^2} k \sum_{s,f,m=0}^{\infty} \frac{|q_f B|}{\omega_{q,k}} \sqrt{k^2 - p_{\perp}^2(q_f, m, s)} \theta(k^2 - p_{\perp}^2(q_f, m, s)) [1 - \theta(\mu - \omega_{q,k})] . \end{aligned} \quad (2.6)$$

Furthermore, if we set $\mu = 0$, the step function in (2.6) vanishes and we obtain the flow equation in the vacuum.

3 Numerical results

Solving the flow equation can in practice be done in two ways. One method is to make a polynomial expansion around the k -dependent minimum and truncate the series, which leads to a set of coupled equations for the coefficients of the terms in this series. The other possibility is to solve the flow equation numerically for the potential $U_k(\phi)$ discretizing the field value ϕ . We will do the latter, but discretizing instead in the quantity $\rho = \frac{\phi^2}{2}$ in the interval $\rho \in [0; 8000]$ (MeV)², using $n = 200$

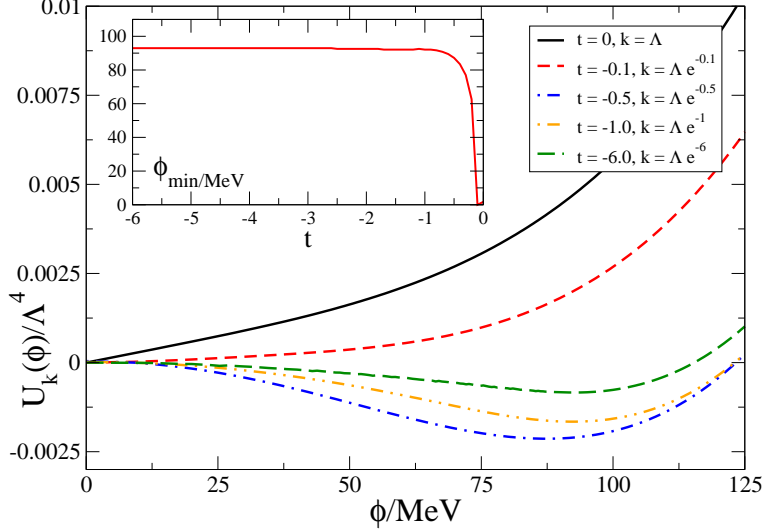


Figure 1. Potential $U_k(\phi)$ for different values of k . Note that the curves do not evolve monotonically in k . The inset shows the minimum $\phi_0 = f_{\pi,k}$ as a function of $t = \log \frac{k}{\Lambda}$.

grid points². The probed interval corresponds to $\phi \in [0; 126.5]$ MeV, which comfortably includes the minimum of the potential.

Earlier we pointed out that $h = h_\Lambda$ and it does not appear in the flow equation (2.5). However, one can show that $h = f_\pi m_\pi^2$ and so a nonzero h is introduced via the boundary condition (2.4) of the effective potential. One must therefore tune the parameters m_Λ and λ_Λ separately for $h = 0$ and $h \neq 0$ to reproduce pion decay constant f_π and the pion mass m_π in the vacuum correctly. After tuning the parameters, the tree level potential $U_\Lambda(\phi)$ is given by Eq. (2.4), with $m_\Lambda^2 = 0$ throughout, and $\lambda_\Lambda = 1.72$ for³ $h = f_\pi m_\pi^2$, and $\lambda_\Lambda = 2.125$ for⁴ $h = 0$. This ensures in both cases that at $T = \mu = B = 0$, the minimum of the potential is at $\phi_0 = f_\pi = 93$ MeV, and that the pion mass is correctly $m_\pi = 140$ MeV for $h > 0$, $h = 0$, respectively. Also the σ mass is in the allowed range of the broad resonance $m_\sigma = 400 - 800$ MeV, and we specifically take $m_\sigma = 450, 480$ MeV, again for $h > 0$ and $h = 0$. We use an ultraviolet cutoff of $\Lambda = 500$ MeV as in Ref. [31]. We checked that changing the cutoff to 800 MeV results in a correction of approximately 3% to T_c at $\mu = 0$, $B = 0$, a precision we expect to persist throughout. The bare coupling of course changes significantly, but the physical result does not.

We ignore the running of the Yukawa coupling and set $g_k = 3.2258$ for all k . This yields a quark mass of $m_q = g\phi_0 = gf_\pi = 300$ MeV. The k -dependent masses $m_{\pi,k}^2$ and $m_{\sigma,k}^2$ are related to the k -dependent minimum $\phi_{0,k} = f_{\pi,k}$ of the effective potential as follows

$$m_{\pi,k}^2 = \left. \frac{\partial^2 U_k}{\partial \phi^2} \right|_{\phi=f_{\pi,k}}, \quad m_{\sigma,k}^2 = m_{\pi,k}^2 + \phi^2 \left. \frac{\partial^2 U_k}{\partial \phi^2} \right|_{\phi=f_{\pi,k}}. \quad (3.1)$$

²We checked that the results were insensitive to using half as many point, $n = 100$.

³We will call this the “ $h > 0$ ” case or physical point.

⁴ $h = 0$ is the chiral limit.

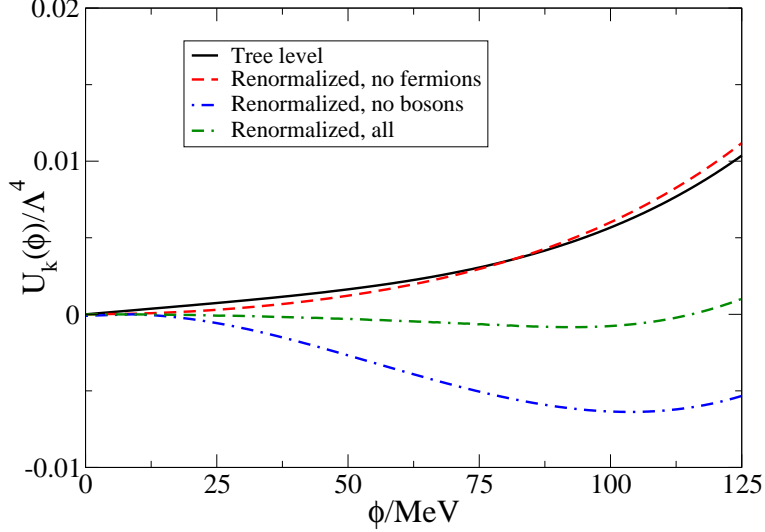


Figure 2. Real part of the effective potential $U_k(\phi)$ for $\mu = T = B = 0$. At tree-level $U_\Lambda(\phi)$ (black) and when fully renormalized $U_{k=0}(\phi)$ (green). The blue and red curves are the effective potential where we have ignored the effects of the bosonic quantum fluctuations and fermionic vacuum fluctuations, respectively.

The physical masses m_π^2 and m_σ^2 are given by evaluating Eq. (3.1) at $k = 0$. Finally, when we integrate the flow equation, we use the dimensionless variable $t \equiv \log \frac{k}{\Lambda}$. Thus $k = \Lambda$ corresponds to $t = 0$ and $k = 0$ corresponds to $t = -\infty$.

In Fig. 1, we show how the potential $U_k(\phi)$ develops for different values of k . The black curve is the tree-level potential, $k = \Lambda$, and the green the full quantum effective potential $U_0(\phi)$. It is interesting to note that the potential at intermediate stages, here shown as red, blue, and orange curves, do not evolve monotonically. This shows that the bosonic and fermionic terms in the flow equation dominate in different regions of integration. It is important to point out that the exact effective potential is both real and convex. It is an artefact of our truncation that the potential becomes nonconvex and that it develops an imaginary part [32].

The inset shows the minimum $\phi_0 = f_{\pi,k}$ as a function of the dimensionless variable t . The minimum converges to f_π around $t = -3$, but other features of the potential, such as the curvature in the potential minimum, continue to develop somewhat later. By $t = -6$ the potential has settled.

In Fig. 2, we show various instances of the quantum effective potential $U_k(\phi)$ for $\mu = T = B = 0$, $h > 0$, i.e. in the vacuum. The black line is the tree level potential $U_{k=\Lambda}(\phi)$ and the green line the fully renormalized effective potential $U_{k=0}(\phi)$. The red/blue lines are also fully renormalized, but ignoring the fermion/boson contribution to the fluctuations. We see that the two pull in opposite directions, enhancing/weakening symmetry breaking. The difference comes basically down to a different sign of the relevant terms in the flow equation (2.6). In some cases, the fermionic quantum fluctuations can destabilize the effective potential altogether. Notice also that the green line is not simply the average of the red and the blue, as the flow equation performs non-linear resummations.

Then in Fig. 3, we show the effective potential for different values of the magnetic field B measured in units of the ultraviolet cutoff Λ^2 , at $T = \mu = 0$, and here shown for $h > 0$. We notice that the

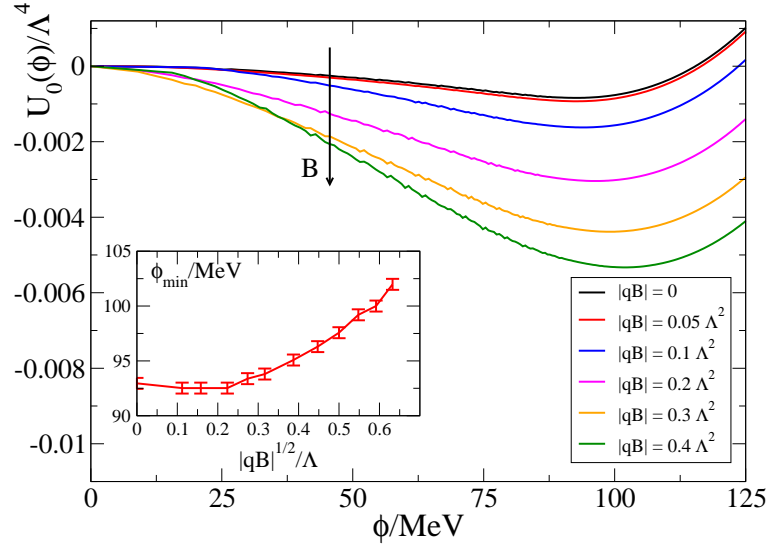


Figure 3. Full quantum effective potential $U_0(\phi)$ for different values of the magnetic field. The arrow indicates the direction of increasing B . Inset shows the minimum ϕ_0 as a function of the magnetic field B with error bars.

effective potential becomes deeper and the minimum moves to the right with increasing B . There is some roughness of the effective potential for ρ to the left of the minimum. The reason is that the potential is complex to the left of the minimum and numerical integration therefore becomes more noisy. We checked that this has no influence on the location of the minimum of the potential. The inset shows the minimum ϕ_0 as a function of the strength of the magnetic field. The minimum is within discretization errors an increasing, but non-linear, function of B . The error bars are meant to represent the resolution of the discretization in ϕ . We found similar behaviour for $h = 0$. This result is in agreement with magnetic catalysis of dynamical symmetry breaking (MCDS) which is the effect that chiral symmetry is broken dynamically for any nonzero magnetic field when it is intact for $B = 0$, and more generally that a nonzero magnetic enhances symmetry breaking. This effect is now well established in fermionic systems in an external magnetic field, see for example Refs. [33–39].

In the left-hand frame of Fig. 4, we show the minimum of the effective potential for $B = \mu = 0$, $h > 0$ as a function of temperature T , allowing for the determination of the critical temperature at this value of the chemical potential. The order parameter goes to zero in a continuous manner which shows that the transition is second order or a cross-over. The finite coarseness of the discretization does not allow us to firmly establish whether it is one or the other. In the right-hand frame we show how this critical temperature depends on the magnetic field B . The dependence is monotonically, but non-linearly increasing. A similar behaviour was observed for $h = 0$.

Our first main result is then shown in Fig. 5, displaying the phase diagram in the μ - T plane in the chiral limit, for a number of different value of the magnetic field B . The dashed lines show the part of the diagram where the transition is a cross-over, and the full lines where it is first order. At small chemical potential, increasing B corresponds to increasing T_c . But interestingly, the lines

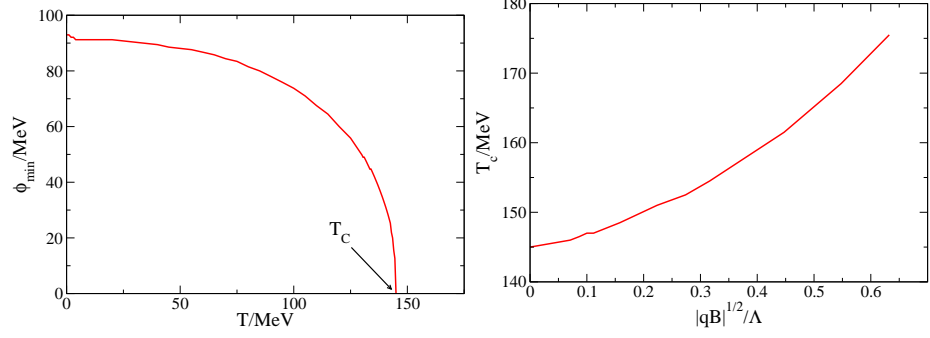


Figure 4. Left: Minimum ϕ of the effective potential for $B = \mu = 0$ at the physical point as a function of temperature T . Right:

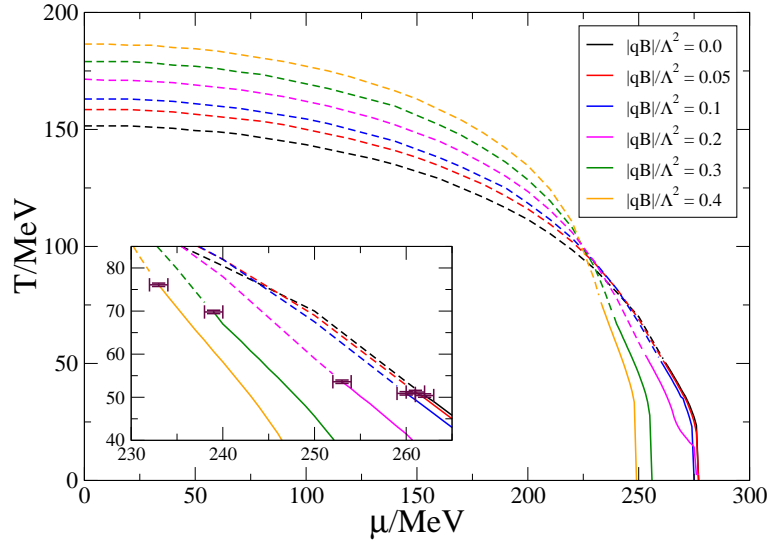


Figure 5. Phase diagram in the μ - T plane in the chiral limit for different values of the magnetic field. The arrows indicate the direction of increasing B .

cross as the large- B curves dip down at much smaller μ_B than the small- B curves. This means that at $\mu \geq 225$ MeV increasing B at fixed μ corresponds to *decreasing* T_c .

At very large chemical potential, the phase transition becomes first order at a critical point (see inset). The crosses indicate the position of these critical points⁵ (T^*, μ^*). Since these appear in the range $\mu \geq 225$ MeV, the curves are ordered such that T^* is an increasing function of B and μ^* is a decreasing function of B .

Additional features in the phase diagram have been reported in [31] at $B = 0$, $h = 0$ and large chemical potential, using slightly different parameters. In this region the authors found that the first-order transition forks into two phase transitions. The left transition line is always of first order

⁵Note that T_c is the temperature at a given μ_B where there is a transition, but is not the temperature at the critical end point.

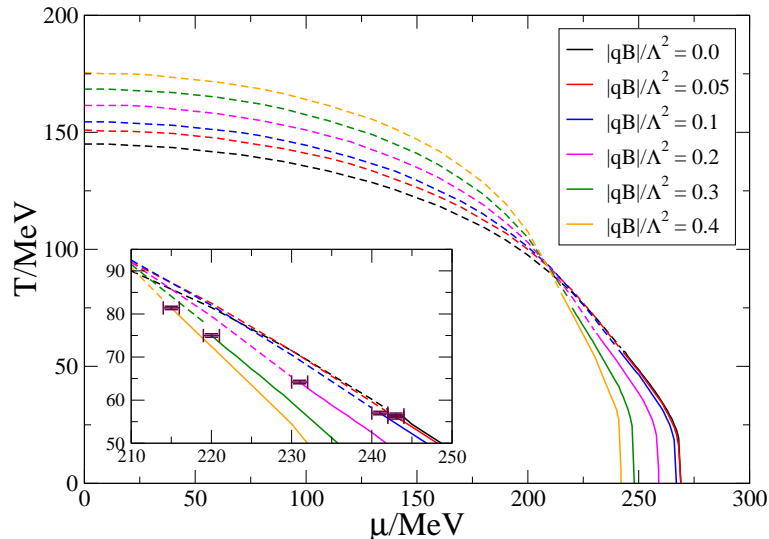


Figure 6. Phase diagram in the μ - T plane at the physical point for different values of the magnetic field. The arrows indicate the direction of increasing B .

while the chiral restoration transition line around the splitting point is initially of first order and turns into a second order transition for lower temperatures.

Although we do see some possible additional structure appearing there, for instance in the $|qB| = 0.2\Lambda^2$ curve, this region seems to be quite sensitive to the discretization of the numerics, and we feel unable to make any firm statements.

In Fig. 6, we show the phase diagram in the μ - T plane, but now at the physical point $h > 0$, again for different values of the magnetic field B . Again, the curves cross, now at a value of around $\mu = 210$ MeV. In the inset, the crosses again indicate the position of the critical points.

4 Discussion and conclusion

In the present paper, we have mapped out the phase diagram of the quark-meson model in the presence of constant external magnetic field using the functional renormalization group. For small values of the chemical potential, our study shows that the critical temperature is an increasing function of the magnetic field B . However, for larger values of μ the curves for different B cross in the $T - \mu$ plane and so the critical temperature becomes a decreasing function of chemical potential for large values of μ . This total inversion of the ordering of the curves takes place within a small range of chemical potentials of about 20 MeV, centered around 225 and 210 MeV for $h = 0$ and $h > 0$, respectively. This behavior has also been seen in the NJL calculations of Refs. [14, 40] and the calculations of Ref. [41] based on holography. The phenomenon was appropriately dubbed “inverse magnetic catalysis” (IMC). Basically, there are two competing effects at work. Increasing the magnetic field B , effectively increases the particle-particle coupling and thereby enhances chiral symmetry breaking [34, 35]. The chemical potential μ tends to split the particles and antiparticles and thus works against chiral symmetry breaking. This is clearly demonstrated in the left half of

Figs. 5 and 6; namely that for fixed μ , the critical temperature increases with B , and for fixed B , the critical temperature decreases with μ . However, for larger values of B , the critical lines are crossing and so the critical temperature decreases with B (and still decreases with μ as well). Thus the effects of increasing the magnetic field must have changed qualitatively - namely that the cost of chiral symmetry breaking exceeds the gain [41].

Another main focus of our study was to pin down the critical endpoint, and its dependence on B . It turned out that the first-order line extends to higher temperatures for larger B ; and because of the overall order-inversion of the transition curves the critical μ decreases with larger B . In particular, the largest magnetic field considered here corresponds to $|qB| \sim 5m_\pi^2$, a value expected to be achievable in heavy-ion collisions. In this case, the critical endpoint should be expected at $(T^*, \mu^*) \simeq (81.4, 215)$ MeV, rather than the $B = 0$ values of $(56.6, 243)$. In particular, this means that the first-order region can be reached at about 10-15 percent smaller baryon density.

In Ref. [21], the authors have determined the phase diagram of QCD in the μ - T plane for $B = 0$ using lattice simulations with physical quark masses and a Taylor-expansion technique around $\mu = 0$. The prediction for the critical line is in reasonable agreement with the present results for small values of the chemical potential but the curves diverge at around $\mu = 150$ MeV. Of course, for some (large) value of the baryon chemical potential, the lattice results can no longer be trusted so the discrepancy is not necessarily worrisome.

D'Elia *et al* have carried out lattice simulations in a constant magnetic background at zero chemical potential [22]. They explored various constituent quark masses corresponding to a pion mass of 200 – 480 MeV and different magnetic fields, up to $|qB| \sim 20 m_\pi^2$ for the lightest quark masses. For these values of the pion mass, they found that there is a slight increase in the critical temperature T_c for the chiral transition. These results have been confirmed by Bali *et al* [24, 25]. The same group has also carried out lattice simulations for physical values of the pion mass, i.e. $m_\pi = 140$ MeV. Their results which are extrapolated to the continuum limit show that the critical temperature is a decreasing function of the magnetic field [24, 25]. Hence the critical temperature for fixed $|qB|$ as a function of the quark mass is nontrivial. Moreover, at $|qB| = 1$ (GeV)² the transition is still a crossover, although somewhat stronger than at $B = 0$. This is in stark contrast to most model calculations that imply an increasing critical temperature as a function of B . This is irrespective of whether one goes beyond mean field or not. Since this discrepancy is not understood, more work is needed to resolve the problem.

Acknowledgments

J. O. A. would like to thank Gunnar Bali, Gergely Endrődi, and Falk Bruckmann for useful discussions on their lattice simulations. The authors would like to thank Andreas Schmitt, Toni Rebhan, Florian Preis, and Marcus Pinto for discussions on the inverse magnetic catalysis. A. T. was supported by the Carlsberg Foundation. J. O. A. thanks the Niels Bohr International Academy and the Discovery Center for kind hospitality during the course of this work.

A Flow equation

In this appendix, we briefly discuss the derivation of the flow equation (2.5). The starting point is the exact flow equation for the k -dependent effective action $\Gamma_k[\phi]$ [28]

$$\partial_k \Gamma_k[\phi] = \frac{1}{2} \text{Tr} \left[\partial_k R_k(q) \left[\Gamma_k^{(2)} + R_k(p) \right]^{-1} \right], \quad (\text{A.1})$$

where the superscript n on $\Gamma_k[\phi]$ means the n th functional derivative of $\Gamma_k[\phi]$ and the trace is over the spacetime momenta p , and indices of the inverse propagator matrix. The function $R_k(p)$ is a regulator and is introduced in order to implement the renormalization group ideas: $R_k(p)$ is large for $p < k$ and small for $p > k$ whenever $0 < k < \Lambda$, and $R_\Lambda(p) = \infty$. These properties ensure that the modes below k are heavy and decouple, and only the modes between k and the UV cutoff Λ are light and integrated out. In order to proceed, we need to choose one regulator for the bosonic fields and one for the fermionic fields. The choice of regulator has been discussed extensively in the literature and in the present work we will use [42, 43]

$$R_k^B(p) = (k^2 - \mathbf{p}^2) \theta(k^2 - \mathbf{p}^2), \quad (\text{A.2})$$

$$R_k^F(p) = \left(\sqrt{\frac{(p_0 + i\mu)^2 + k^2}{(p_0 + i\mu)^2 + \mathbf{p}^2}} - 1 \right) (\not{p} + i\mu\gamma^0) \theta(k^2 - \mathbf{p}^2). \quad (\text{A.3})$$

This regulator is very convenient in practical calculations since one can carry out the integral over three-momenta exactly. This turns the flow equation into a partial differential equation as we show below.

The derivate expansion of the full quantum effective action reads

$$\begin{aligned} \Gamma[\phi] = \int_0^\beta d\tau \int d^3x \left\{ \frac{1}{2} Z_k^{(1)} [(\nabla\sigma)^2 + (\nabla\boldsymbol{\pi})^2] + \frac{1}{2} Z_k^{(2)} [(\partial_0\sigma)^2 + (\partial_0\boldsymbol{\pi})^2] \right. \\ \left. + \dots + \dots U_k(\phi) + Z_k^{(3)} \bar{\psi} [\gamma_0 \partial_0 - \gamma_4 \mu] \psi + Z_k^{(4)} \bar{\psi} \gamma_i \partial_i \psi + g_k \bar{\psi} [\sigma - i\gamma_5 \boldsymbol{\tau} \cdot \boldsymbol{\pi}] \psi + \dots \right\}, \quad (\text{A.4}) \end{aligned}$$

where $Z_k^{(i)}$ are wavefunction renormalization constants, $U_k(\phi)$ is the scale-dependent effective potential, and the ellipsis denote higher-order derivative terms that satisfy the symmetries of the effective action. Note that the $Z_k^{(i)}$ are in principle different since Lorentz invariance is broken due to both finite temperature and finite density. In the local-potential approximation, one neglects the scale dependence of $Z_k^{(i)}$ and retain their tree-level values $Z_k^{(i)} = 1$. The flow equation then reduces to a coupled equation for the effective potential $U_k(\phi)$ and the Yukawa coupling g_k . If we furthermore ignore the running of the latter, we obtain a tractable equation for the former. Ignoring the running of the Yukawa coupling, implies that the approximation does not correspond to the local-potential approximation [31].

The effective potential $U_k(\phi)$ is defined by evaluating the effective action $\Gamma_k[\phi]$ for space-time independent fields and dividing by the VT , where V is the volume:

$$U_k(\phi_{\text{uni}}) = \frac{1}{\beta V} \Gamma_k[\phi_{\text{uni}}]. \quad (\text{A.5})$$

In the following, we neglect the subscript uni. Inserting Eq. (A.5) into Eq. (A.1), we obtain the flow equation for U . This yields

$$\begin{aligned} \partial_k U_k = & \frac{1}{2} \mathbb{J}_P \text{Tr} \left\{ \partial_k R_k^B(p) \left[(p^2 + R_k^B(p)) \delta_{ij} + \frac{\partial^2 U_k}{\partial \Phi_i \partial \Phi_j} \right]^{-1} \right\} \\ & + \frac{1}{2} \mathbb{J}_{\{P\}} \text{Tr} \left\{ \partial_k R_k^F(p) [\mathcal{P} - \gamma_4 \mu + g\phi + R_k^F(p)]^{-1} \right\}, \end{aligned} \quad (\text{A.6})$$

where $\Phi = (\sigma, \boldsymbol{\pi})$, $i, j = 1, 2, 3, 4$, and the trace is over internal indices only. The symbols \mathbb{J}_P and $\mathbb{J}_{\{P\}}$ are defined by

$$\mathbb{J}_P = T \sum_{P_0=2\pi nT} \int \frac{d^3 p}{(2\pi)^3}, \quad (\text{A.7})$$

$$\mathbb{J}_{\{P\}} = T \sum_{P_0=(2n+1)\pi T} \int \frac{d^3 p}{(2\pi)^3}. \quad (\text{A.8})$$

Using the chain rule, the matrix appearing in the first term in Eq. (A.6)

$$\begin{pmatrix} p^2 + R_k^B(p) + U'_k + U''_k & 0 & 0 & 0 \\ 0 & p^2 + R_k^B(p) + U'_k & 0 & 0 \\ 0 & 0 & p^2 + R_k^B(p) + U'_k & 0 \\ 0 & 0 & 0 & p^2 + R_k^B(p) + U'_k \end{pmatrix}, \quad (\text{A.9})$$

where $U'_k = \frac{\partial U_k}{\partial \rho}$ with $\rho = \frac{1}{2}\phi^2$. We notice that the matrix Eq. (A.9) is simply the inverse tree-level propagator if we make the substitution $\mathcal{V}_0 \rightarrow U_k + R_k^B(p)$. Integration over \mathbf{p} gives

$$\begin{aligned} \partial_k U_k = & \frac{k^4}{12\pi^2} T \sum_{n=-\infty}^{\infty} \left[\frac{3}{\omega_n^2 + k^2 + U'_k} + \frac{1}{\omega_n^2 + k^2 + U'_k + 2\rho U''_k} \right] \\ & - \frac{N_c N_f k^4}{6\pi^2} T \sum_{n=-\infty}^{\infty} \left[\frac{1}{(\omega_n + i\mu)^2 + k^2 + m_q^2} \frac{1}{(\omega_n - i\mu)^2 + k^2 + m_q^2} \right]. \end{aligned} \quad (\text{A.10})$$

Summing over the Matsubara frequencies, we obtain

$$\begin{aligned} \partial_k U_k = & \frac{k^4}{12\pi^2} \left\{ \frac{3}{\omega_{1,k}} [1 + 2n_B(\omega_{1,k})] + \frac{1}{\omega_{2,k}} [1 + 2n_B(\omega_{2,k})] \right\} \\ & - \frac{N_c N_f k^4}{3\pi^2} \left\{ \left[\frac{1}{\omega_{q,k}} (1 - n_F^+(\omega_{q,k}) - n_F^-(\omega_{q,k})) \right] \right\}, \end{aligned} \quad (\text{A.11})$$

where $\omega_{1,k} = \sqrt{k^2 + U'_k}$, $\omega_{2,k} = \sqrt{k^2 + U'_k + \phi^2 U''_k}$, $\omega_{q,k} = \sqrt{k^2 + g^2 \phi^2}$, $N_B(x) = 1/(e^{\beta x} - 1)$. and $N_F^\pm(x) = 1/(e^{\beta(x \pm \mu)} + 1)$.

We next briefly consider the flow equation in a constant magnetic field B [10]. As we pointed out above, the matrices appearing on the right-hand side of the flow equation are essentially the inverse tree-level propagators. We can therefore find the flow equation in a constant magnetic background

since the tree-level propagators are expressed in terms of the well-known solutions to the Klein-Gordon and Dirac equations in constant B field. The spectra are given by $E^2 = p_z^2 + (2m+1)|qB|$ for bosons and $E^2 = p_z^2 + (2m+1-s)|q_f B|$ for fermions, where q_z is the z -component of the three-momentum, m is the m th Landau level and $s = \pm 1$ is the spin variable. We therefore make the substitutions $\mathbf{q}^2 \rightarrow q_z^2 + (2m+1)|qB|$ and $q_z^2 + (2m+1-s)|q_f B|$ in the regulators (A.2) and (A.3). In the case of the charged particles the sum-integral is replaced by a sum over Matsubara frequencies $P_0 = 2\pi nT$, a sum over Landau levels m , and an integral over momenta p_z in $d = 1$ dimension:

$$\oint_P \rightarrow \frac{|qB|T}{2\pi} \sum_{P_0=2n\pi T} \sum_{m=0}^{\infty} \int \frac{dp_z}{2\pi}, \quad (\text{A.12})$$

$$\oint_{\{P\}} \rightarrow \frac{|qB|T}{2\pi} \sum_{P_0=(2n+1)\pi T} \sum_{m=0}^{\infty} \int \frac{dp_z}{2\pi}. \quad (\text{A.13})$$

After integrating over p_z and summing over Matsubara frequencies, one obtains.

$$\begin{aligned} \partial_k U_k = & \frac{k^4}{12\pi^2} \left[\frac{1}{\omega_{1,k}} (1 + 2n_B(\omega_{1,k})) + \frac{1}{\omega_{2,k}} (1 + 2n_B(\omega_{2,k})) \right] \\ & + \frac{|qB|}{2\pi^2} \sum_{m=0}^{\infty} \frac{k}{\omega_{1,k}} \sqrt{k^2 - p_{\perp}^2(q, m, 0)} \theta(k^2 - p_{\perp}^2(q, m, 0)) [1 + 2n_B(\omega_{1,k})] \\ & - \frac{N_c}{2\pi^2} \sum_{s,f,m=0}^{\infty} \frac{|q_f B|k}{\omega_{q,k}} \sqrt{k^2 - p_{\perp}^2(q_f, m, s)} \theta(k^2 - p_{\perp}^2(q_f, m, s)) [1 - n_F^+(\omega_{q_f,k}) - n_F^-(\omega_{q_f,k})], \end{aligned} \quad (\text{A.14})$$

where we have defined $p_{\perp}^2(q, m, s) = (2m+1-s)|qB|$. We close the Appendix by taking the limit $B \rightarrow 0$ in Eq. (A.14). We change variable $p_{\perp}^2 = 2|qB|m$, which yields $p_{\perp} dp_{\perp} = |qB|dm$. Replacing the sum by an integral, we obtain

$$\begin{aligned} \partial_k U_k = & \frac{k^4}{12\pi^2} \left[\frac{1}{\omega_{1,k}} (1 + 2n_B(\omega_{1,k})) + \frac{1}{\omega_{2,k}} (1 + 2n_B(\omega_{2,k})) \right] \\ & + \frac{k}{2\omega_{1,k}\pi^2} \int_0^{\infty} dp_{\perp} p_{\perp} \sqrt{k^2 - p_{\perp}^2} \theta(k^2 - p_{\perp}^2) [1 + 2n_B(\omega_{1,k})] \\ & - \frac{N_c N_f k}{\omega_{q,k}\pi^2} \int_0^{\infty} dp_{\perp} p_{\perp} \sqrt{k^2 - p_{\perp}^2} \theta(k^2 - p_{\perp}^2) [1 - n_F^+(\omega_k) - n_F^-(\omega_{q,k})]. \end{aligned} \quad (\text{A.15})$$

Finally, integrating over p_{\perp} , the flow equation (A.15) reduces to Eq. (A.11).

References

- [1] M. G. Alford, A. Schmitt, K. Rajagopal, and T. Schäfer, *Color superconductivity in dense quark matter*, *Rev. Mod. Phys.* **80** (2008) 1455 arXiv:0709.4635 [hep-ph] [SPIRES].
- [2] K. Fukushima and T. Hatsuda, *The phase diagram of QCD Rept. Prog. Phys.* **74** (2011) 014001 arXiv:1005.4814 [hep-ph] [SPIRES].

- [3] J. M. Lattimer and M. Prakash *Neutron Star observations: Prognosis for equation of state constraints*, *Phys. Rept.* **442** (2007) 109 [astro-ph/0612440] [SPIRES].
- [4] D. E. Kharzeev, L. D. McLerran, and H. J. Warringa, *The effects of topological charge change in heavy ion collisions: “Event by event P and CP violation”*, *Nucl. Phys. A* **803** (2008) 227 [arXiv:0711.0950] [SPIRES].
- [5] V. Skokov, A. Y. Illarionov, and V. Toneev, *Estimate of the magnetic field strength in heavy-ion collisions*, *Int. J. Mod.Phys. A* **24** (2009) 5925 [arXiv:0907.1396] [SPIRES].
- [6] A. Bzdak and V. Skokov, *Event-by-event fluctuations of magnetic and electric fields in heavy ion collisions*, arXiv:1111.1949 [hep-ph] [SPIRES].
- [7] N. O. Agasian and S. M. Fedorov, *Quark-hadron phase transition in a magnetic field*, *Phys. Lett. B* **663** (2008) 445, [arXiv:0803.3156] [SPIRES].
- [8] A. J. Mizher, M. N. Chernodub, and E. S. Fraga, *Phase diagram of hot QCD in an external magnetic field: possible splitting of deconfinement and chiral transitions*, *Phys. Rev. D* **82** (2010) 105016 [arXiv:1004.2712] [SPIRES].
- [9] J. O. Andersen and R. Khan, *Chiral transition in a magnetic field and at finite baryon density* *Phys. Rev. D* **85** (2012) 065026 [arXiv:1105.1290] [SPIRES].
- [10] V. Skokov, *Phase diagram in an external magnetic field beyond a mean-field approximation* *Phys. Rev. D* **85** (2012) 034026 [arXiv:1112.5137] [SPIRES].
- [11] V. Skokov, B. Friman, E. Nakano, K. Redlich, and B.-J. Schaefer. *Vacuum fluctuations and the thermodynamics of chiral models* *Phys. Rev. D* **82** (2010) 034029 [arXiv:1005.3166] [SPIRES].
- [12] J. O. Andersen, R. Khan, and L. T. Kyllingstad, *The chiral phase transition and the role of vacuum fluctuations*, [arXiv:1102.2779] [SPIRES].
- [13] E. S. Fraga and A. J. Mizher, *Chiral transition in a strong magnetic background*, *Phys. Rev. D* **78** (2008) 025016 [arXiv:0804.1452] [SPIRES].
- [14] S. S. Avancini, D. P. Menezes, M. B. Pinto, and C. Providencia, *The QCD critical end point under strong magnetic fields*, arXiv:1202.5641 [SPIRES].
- [15] K. Fukushima, M. Ruggieri, and R. Gatto *Chiral magnetic effect in the PNJL model* *Phys. Rev. D* **81** (2010) 114031 [arXiv:1003.0047] [SPIRES].
- [16] Sh. Fayazbakhsh and N. Sadooghi, *Phase diagram of hot magnetized two-flavor color superconducting quark matter* *Phys. Rev. D* **83** (2011) 025026 [arXiv:1009.6125] [SPIRES].
- [17] R. Gatto and M. Ruggieri, *Dressed Polyakov loop and phase diagram of hot quark matter under magnetic field*, *Phys. Rev. D* **82** (2010) 054027 [arXiv:1007.0790] [SPIRES]; *Deconfinement and chiral symmetry restoration in a strong magnetic background* *ibid* **83** (2011) 034016 [arXiv:1012.1291] [SPIRES].
- [18] K. Kashiwa, *Entanglement between chiral and deconfinement transitions under strong uniform magnetic background field*, *Phys. Rev. D* **83** (2011) 117901, [arXiv:1104.5167] [SPIRES].
- [19] D. C. Duarte, R. L. S. Farias, and R. O. Ramos, *Optimized perturbation theory for charged scalar fields at finite temperature and in an external magnetic field*, *Phys. Rev. D* **84** (2011) 083525 [arXiv:1108.4428] [SPIRES].
- [20] J. O. Andersen, *Thermal pions in a magnetic background*, [arXiv:1202.2051] [SPIRES].

- [21] G. Endrődi, Z. Fodor, S. D. Katz, and K. K. Szabo *JHEP* **1007** (2011) 001 [arXiv:1102.1356][SPIRES].
- [22] M. D’Elia, S. Mukherjee, and F. Sanfilippo, *QCD phase transition in a strong magnetic background*, *Phys. Rev. D* **82**, (2010) 051501(R) [arXiv:1005.5365] [SPIRES].
- [23] M. D’Elia and F. Negro, *Chiral properties of strong interactions in a magnetic background*, *Phys. Rev. D* **83** (2011) 114028 [arXiv:1103.2080] [SPIRES].
- [24] G. S. Bali, F. Bruckmann, G. Endrődi, Z. Fodor, S. D. Katz, S. Krieg, A. Schafer, and K. K. Szabo, *The QCD phase diagram for external magnetic fields*, *JHEP* **1202** (2012) 044 [arXiv:1111.4956] [SPIRES].
- [25] G. S. Bali, F. Bruckmann, G. Endrődi, Z. Fodor, S.D. Katz, and A. Schafer, *QCD quark condensate in external magnetic fields* [arXiv:1206.4205] [SPIRES]; G. Bali, G. Endrődi, and F. Bruckmann, Private communications.
- [26] E. S. Fraga and L. F. Palhares, *Deconfinement in the presence of a strong magnetic background: an exercise within the MIT bag model* [arXiv:1201.5881] [SPIRES].
- [27] K. Fukushima, *Chiral effective model with the Polyakov loop*, *Phys. Lett. B* **591**, (2004) 277 [hep-ph/0310121] [SPIRES].
- [28] C. Wetterich, *Average action and the renormalization group equations*, *Nucl. Phys. B* **352** (1991) 529.
- [29] G. ’t Hooft *How Instantons solve the U(1) problem*, *Phys. Rep.* **142** 357 (1986).
- [30] O. Rosten, *Fundamentals of the exact renormalization group*, *Phys. Rept.* **511** 4 (2012) 177 [arXiv:1003.1366] [SPIRES].
- [31] B.-J. Schaefer and J. Wambach, *The Phase diagram of the quark meson model*, *Nucl. Phys. A* **757** (2005) 479 [nucl-th/0403039] [SPIRES].
- [32] J. Berges, N. Tetradis, and C. Wetterich, *Nonperturbative renormalization group flow in quantum field theory and statistical physics*, *Phys. Rept.* **363** (2002) 223 [hep-ph/0005122].
- [33] K. G. Klimenko, *Three-dimensional Gross-Neveu model at nonzero temperature and in an external magnetic field* *Z. Phys. C* **54** (1992) 323.
- [34] V. P. Gusynin, V. A. Miransky, and I. A. Shovkovy, *Catalysis of dynamical flavor symmetry breaking by a magnetic field in (2+1)-dimensions*, *Phys. Rev. Lett.* **73** (1994) 3499 [hep-ph/9405262] [SPIRES].
- [35] V. P. Gusynin, V.A. Miransky, and I.A. Shovkovy, *Dimensional reduction and catalysis of dynamical symmetry breaking by a magnetic field*, *Nucl. Phys. B* **462** (1996) 249 [hep-ph/9509320] [SPIRES].
- [36] C. N. Leung, Y. J. Ng, and A. W. Ackley, *Schwinger-Dyson equation approach to chiral symmetry breaking in an external magnetic field*, *Phys. Rev. D* **54**, 4181 (1996); *Chiral symmetry breaking in a uniform external magnetic field* *ibid D* **55** (1997) 6504 [hep-th/9701172] [SPIRES] .
- [37] D. Ebert, K. G. Klimenko, M. A. Vdovichenko, and A. S. Vshivtsev, *Magnetic oscillations in dense cold quark matter with four fermion interactions*, *Phys.Rev. D*, **61** (2000) 025005 [hep-ph/9905253] [SPIRES].
- [38] C.N. Leung, S.-Y. Wang, *Gauge independent approach to chiral symmetry breaking in a strong magnetic field*, *Nuclear Physics B* **747** (2006) 266 [hep-ph/0510066] [SPIRES].
- [39] E. J. Ferrer and V. de la Incera, *Magnetic catalysis in the presence of scalar fields*, *Phys. Lett. B.* **481** (2000) 287 [hep-ph/0004113] [SPIRES] ; *Dynamically Generated Anomalous Magnetic Moment in Massless QED*, *Nuclear Physics B* **824** (2010) 217 [arXiv:0905.1733] [SPIRES].
- [40] T. Inagaki, D. Kimura, and T. Murata, *Four-Fermion Interaction Model in a Constant Magnetic Field*

at Finite Temperature and Chemical Potential 111 (2004) 371 [hep-ph/0312005] [SPIRES].

- [41] F. Preis, A. Rebhan, and A. Schmitt *Inverse magnetic catalysis in dense holographic matter* *JHEP* 1103 (2011) 033 [arXiv:1012.4785] [SPIRES].
- [42] D. Litim, *Optimized renormalization group flows*, *Phys. Rev. D* **64** (2001) 105007 [hep-th/0103195] [SPIRES].
- [43] B. Stokic, B. Friman and K. Redlich, *The Functional Renormalization Group and $O(4)$ scaling*, *Eur. Phys. J. C* **67** (2010) 425 [arXiv:0904.0466] [SPIRES].